JOURNAL OF SPACECRAFT AND ROCKETS
Vol. 33, No. 4, July–August 1996

Experimental and Computational Wake Structure Study for a Wide-Angle Cone

A. Danckert* and H. Legge†
DLR, German Aerospace Research Establishment, D-37073 Göttingen, Germany

The establishment of a vortex in highly nonequilibrium flow (non-Maxwellian distribution function of the translational degrees of freedom) in the wake of a 70-deg blunted cone under rarefied hypersonic conditions is investigated numerically by the direct simulation Monte Carlo method and experimentally by Patterson probe measurements. The experiments give detailed information on the molecular number fluxes. The experimental results are compared to the calculations, which give even more detailed information on the molecular distribution function. A vortex is formed in the wake of the cone for the two freestream conditions considered. On the axis of symmetry, the molecular distribution function can be approximated by an ellipsoidal one.

Nomenclature

Kn	= Knudsen number
k	= Boltzmann constant, J/K
M	= Mach number
N_f	= ratio of real to model molecule number
N_s	= number of model molecules in simulation cell
n	= number density, m^{-3}
$\dot{n}_i$	= incoming number flux at entrance plane of Patterson probe, $m^{-2}s^{-1}$
$\dot{n}_o$	= outgoing number flux at exit plane of Patterson probe, $m^{-2}s^{-1}$
p	= pressure, bar
R	= gas constant for N_2, J/(K · kg)
S	= molecular speed ratio
T	= temperature, K
u	= flow velocity, m/s
V_c	= simulation cell volume
v_k	= velocity of model molecule with label k
v_x, v_y, v_z	= Cartesian velocity components, m/s
W_i, W_o	= transmission probabilities for incoming, outgoing number fluxes
x, y, z	= Cartesian coordinates with origin at model nose, mm
α	= angle with respect to opposite flow direction, deg
Θ	= characteristic function (i.e., 0 for negative, 1 for positive arguments)
λ	= mean free path, mm
ν	= normal of surface element
ϕ	= turning angle of Patterson probe, counted from negative x direction, deg

Subscripts

D	= dummy probe condition
e	= ellipsoidal distribution
I	= ionization gauge condition
P	= Patterson probe condition
W	= wall condition
0	= stagnation condition
∞	= freestream condition
$\parallel, \perp$	= directions parallel, perpendicular to flow direction

Received Sept. 1, 1995; revision received Jan. 2, 1996; accepted for publication Jan. 3, 1996.

*Research Scientist, Institute for Fluid Mechanics, Bunsenstrasse 10.
†Research Scientist, Institute for Fluid Mechanics, Bunsenstrasse 10. Senior Member AIAA.

Introduction

A GENERIC aeroassist space transfer vehicle (ASTV) configuration, i.e., a 70-deg blunted cone, is being investigated numerically and experimentally by several groups. The wind-tunnel experiments are being conducted both in the United States and Europe. The overall activity is part of an ongoing AGARD fluid dynamic panel Working Group 18 activity focusing on hypersonic flow problems. Initial results are reviewed.[1]

The present investigation is part of an experimental and numerical study at the DLR Göttingen on different aspects, e.g., rarefaction effects, heat-transfer studies, and wake studies, in different wind tunnels including vacuum wind tunnels VXG[2] and the high-enthalpy wind tunnel HEG.[3] This paper focuses on the establishment of a vortex in the wake of the body in rarefied flow. The flow is examined experimentally by a Patterson probe and numerically by the direct simulation Monte Carlo (DSMC) method of Bird.[4]

Experimental Setup and Conditions

The exact geometry of the 70-deg blunted cone model with base diameter $d_b = 50$ mm, nose radius $r_n = 0.25\,d_b$, and corner radius $r_c = 0.025\,d_b$ is described in Ref. 5. The cone (without sting) was suspended by three thin tungsten wires fixed at the backside. The experiments were conducted in the continuously running vacuum wind tunnel V2G, which has a 15-deg half-angle conical nozzle and a test section diameter of 40 cm. The coordinate system and the Patterson probe geometry are given in Fig. 1, where x is the distance on the wake centerline from the model nose. The Patterson probe could be moved in x and y directions and could be turned 360 deg around the slit (not the probe axis), where the slit center was located at $x_P, y_P, z_P = 0$. A dummy probe of the same outer geometry as the Patterson probe could be moved separately to the location $x_D, y_D, z_D = 0$ in the test section to investigate its influence on the flowfield through the Patterson probe reading. The temperature T_P of the Patterson probe and the temperature T_I at the ionization pressure gauge for the range $10^{-5} \le p_I \le 1$ mbar were measured by thermocouples. The gauge and its surrounding stainless-steel vessel were heated to 500 K for outgassing.

Two stagnation/freestream conditions with N_2 as test gas are considered as detailed in Table 1. Test conditions are identified by p_0 in later figures.

Table 1 Stagnation/freestream conditions

p_0, bar	10	2
T_0, K	775	575
T_W, K	635 ± 50	490 ± 50
M	16.83	15.62
n_∞, m^{-3}	3.70×10^{21}	1.44×10^{21}
u_∞, m/s	1258	1082
Kn_∞	2.63×10^{-3}	6.56×10^{-3}

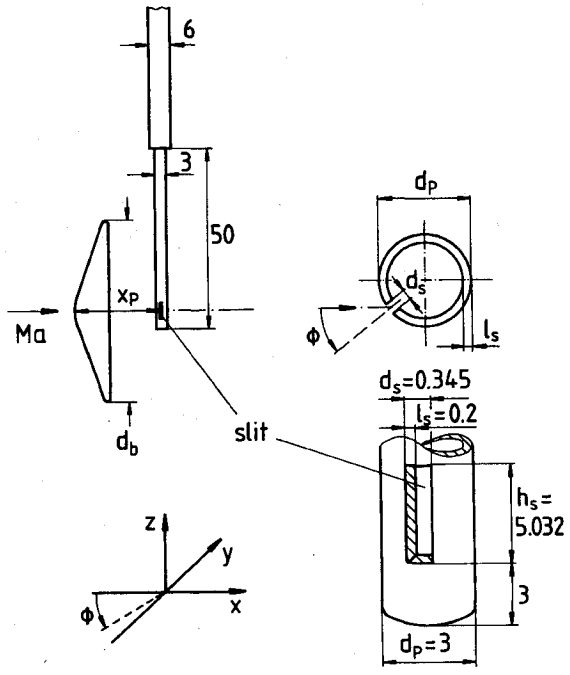

Fig. 1 Model and Patterson probe geometry: dimensions in millimeters.

Theory of Patterson Probe Measurements

The theory of the Patterson probe is treated in a number of papers, e.g., Refs. 6–8. Some aspects are considered in the following, where complete accommodation and a constant probe wall temperature T_P are assumed. The pressure p_P in the probe is established by the particle flux balance between incoming molecules ($\dot{n}_i$) at the entrance plane and outgoing molecules ($\dot{n}_o$) at the exit plane of the slit with the corresponding transmission probabilities W_i and W_o, respectively. This balance leads to the Patterson probe equation

$$p_P/\sqrt{T_P} = \dot{n}_i \times k \times \sqrt{2\pi R} \times (W_i/W_o) \tag{1}$$

where in the present study the value of $p_P/\sqrt{(T_P)}$ was calculated[9] by the corresponding value at the ionization gauge taking into account the effect of pseudothermal transpiration.[10]

For a Maxwellian distribution and free molecular flow around the probe, we obtain

$$\dot{n}_i = (n/2\sqrt{\pi}) \times (u/S) \times \chi(S\cos\alpha) \tag{2}$$

with the definition

$$\chi(S\cos\alpha) = e^{-S^2\cos^2\alpha} + \sqrt{\pi}S\cos\alpha \times [1 + \mathrm{erf}(S\cos\alpha)] \tag{3}$$

In this case, the maximum of $\dot{n}_i$ is at $\alpha = 0$ deg.

An approximation for nonequilibrium distributions, which are symmetric in α and which allow the appearance of two maxima in the number flux as a function of α, can be made by an ellipsoidal distribution function f_e with temperatures $T_\parallel$ and $T_\perp$, parallel and perpendicular to the local flow direction.[11] If this is the x direction, we have

$$f_e = \frac{n}{\sqrt{T_\parallel T_\perp}(2\pi R)^{\frac{3}{2}}} \exp\left(-\frac{(v_x-u)^2}{2RT_\parallel} - \frac{v_y^2}{2RT_\perp} - \frac{v_z^2}{2RT_\perp}\right) \tag{4}$$

This distribution function results in

$$\dot{n}_i = (n/2\sqrt{\pi}) \times (u/S_e) \times \chi(S_e\cos\alpha) \tag{5}$$

with

$$S_e = \frac{1}{\sqrt{\cos^2\alpha/S_\parallel^2 + \sin^2\alpha/S_\perp^2}} \tag{6}$$

$$S_\perp = \frac{u}{\sqrt{2RT_\perp}}, \qquad S_\parallel = \frac{u}{\sqrt{2RT_\parallel}} \tag{7}$$

In general, the transmission probabilities W_i and W_o depend on the given probe geometry and on the molecular distribution function. For circular orifices and a Maxwellian distribution function, numerical results are given in Ref. 7. These results may be used to judge qualitatively the influence of W_i and W_o on the measurements even in the case of a non-Maxwellian (e.g., ellipsoidal) distribution function and to give a quantitative estimation for a slit geometry when the radius of the orifice is replaced by the slit diameter.[12] Appropriate results for the present slit geometry show that the assumption $W_i/W_o = 1$ leads to errors that decrease with decreasing speed ratio and become smaller than about ±10% for speed ratio values less than 1. Since such low values can be expected in the near wake region of the cone (especially near the free stagnation point), where the measurements were performed, we have set $W_i/W_o = 1$ for the present data evaluation.

Then, the evaluation of Eq. (5) at $\alpha = 0$, 90, and 180 deg and the use of Eq. (1) yields

$$\frac{p_P(\alpha=0)}{p_P(\alpha=180)} = \frac{\chi(S_\parallel)}{\chi(-S_\parallel)} \tag{8}$$

and

$$\frac{p_P(\alpha=0)}{p_P(\alpha=90)} = \frac{S_\perp}{S_\parallel} \times \chi(S_\parallel) \tag{9}$$

which enables the determination of $S_\parallel$ and $S_\perp$ from the measured values of p_P. The incoming number flux $\dot{n}_i$ and the product $n \times u$ for an ellipsoidal distribution function are given by Eq. (1) and

$$n \times u = \dot{n}_i(\alpha=0) \times 2 \times \sqrt{\pi} \times \frac{S_\parallel}{\chi(S_\parallel)} \tag{10}$$

DSMC Calculations

The numerical study of the wake structure in the nonreacting rarefied flow was performed with the DSMC method,[4] where the flow dynamics is modeled by following a representative number of model molecules. We used a modified version of the DSMC code MONACO,[13] where the molecular elastic and inelastic collisions were modeled using the variable hard sphere[4] model with standard parameters for a cold nitrogen flow and the Borgnakke–Larsen model[14,15] with fixed rotational and vibrational relaxation numbers of 5 and 50, respectively. At the wall of the cone, complete accommodation was assumed.

To compare the DSMC results directly with the measurements, the inward number flux through a small surface element with surface normal ν within a computational cell of volume V_c containing N_s model molecules (each representing N_f real molecules) was sampled by

$$\dot{n}_i(\nu) = \frac{N_f}{V_c} \sum_{k=1}^{N_s} |\nu \times v_k| \Theta(-\nu \times v_k) \tag{11}$$

In the derivation of this expression the exact positions of the model molecules within the considered cell have been ignored, which should give reasonable approximations for the number flux defined by a surface element (e.g., a part of the orifice of a Patterson probe) with finite linear dimensions in the order of the corresponding cell dimensions. The length of the Patterson probe slit ($h_s \approx 5$ mm) was in the order of several linear cell dimensions, and so the total number flux through the whole entrance plane of the slit was calculated by averaging the sampled number flux (11) over the slit length. The two velocity components $v_{y,k}$ and $v_{z,k}$ appearing in Eq. (11) are determined by a suitable transformation of the sampled radial and circumferential velocity components depending on the azimuth angle of the location of the surface element.

The ellipsoidal velocity-distribution function (4) is of the form

$$f_e(v_x, v_y, v_z) = f_x(v_x) f_y(v_y) f_z(v_z) \tag{12}$$

which implies that the three velocity components are mutually uncorrelated. The reduced distribution functions f_x, f_y, and f_z can be approximately calculated in the DSMC procedure by

$$f_j(v_j) \approx (N_f/V_c)(1/N_s)N[v_j \in (v_j, v_j + \Delta v_j)]$$
$$(j = x, y, z) \quad (13)$$

where $N[v_j \in (v_j, v_j + \Delta v_j)]$ is the sampled number of model molecules in the cell with corresponding velocity component within the denoted range.

Results and Discussion

Influence of the Dummy Probe

A severe handicap of Patterson probe measurements is that the flow can be disturbed by the probe itself. To obtain the magnitude of the disturbances, a dummy probe of the same shape as the Patterson probe was additionally mounted.

For the case $p_0 = 10$ bar, Fig. 2 demonstrates the influence of the dummy probe on the flux ratio ϕ profile, which is the number flux $\dot{n}_i$ normalized with the freestream flux $n_\infty \times u_\infty$ as a function of the turning angle ϕ. The dummy probe was either located opposite to the Patterson probe or at a large distance from the cone, where there should be no significant influence. The comparison between the two resulting profiles shows that at $\phi = 270$ deg, where the slit of the Patterson probe is looking into the direction of the dummy probe location, the influence is the largest, and at $\phi = 90$ deg, when it is looking away, it is the smallest. This indicates that the influence is also for $p_0 = 10$ bar (which is a relative dense case) dominated by direct scattering from the dummy probe to the Patterson probe and by first collisions in the flowfield. Nevertheless, the whole flowfield is altered by the dummy probe and, therefore, also by the Patterson probe, especially in this $p_0 = 10$-bar case where the density is large enough that a strong vortex is established (see later results). The main effect of the dummy probe at $x_D = 15$ mm is an increase of $\dot{n}_i$ for all ϕ (because of an increase in p or n). The main shape of the ϕ profile and thereby of the vortex seems to be conserved, i.e., the maxima and the minima of $\dot{n}_i$ are found still at similar ϕ values for the disturbed and undisturbed profiles. The corresponding investigation for $p_0 = 2$ bar gives similar results.[9]

The measurements show that there can be a severe influence by the dummy probe, but these disturbances are caused by both probes, which might interfere with each other. A small shifting of the vortex center already would have a large effect on the Patterson probe reading in the neighborhood of the vortex center. Further, if the Patterson probe is in the wake of the dummy probe and the disturbance is traveling with the flow to the Patterson probe, the Patterson probe could see the undisturbed flow without the dummy probe. Thus, the Patterson probe could disturb its own reading much less than the dummy probe, and the disturbance by the dummy probe gives an upper limit.

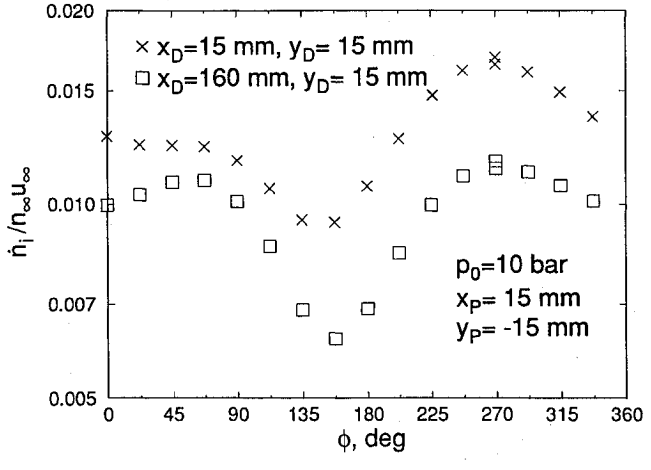

Fig. 2 Influence of dummy probe location on the flux ratio ϕ profile.

Flux Profiles on Wake Centerline

In the following the measured number flux profiles will be directly compared to the corresponding fluxes sampled by use of Eq. (11) in the DSMC calculations with the assumption $W_i/W_o = 1$. First, the calculated streamlines in the near wake region of the blunted cone are shown in Fig. 3. In both cases, a vortex flow has been established, which is more pronounced for $p_0 = 10$ bar. In Fig. 4, the normalized values of n and u and the mean free path on the wake centerline are plotted vs x. The free stagnation point where $u = 0$ is approximately found at $x \approx 22$ mm for $p_0 = 2$ bar and $x \approx 30$ mm for $p_0 = 10$ bar, where in the latter case the stronger vortex flow is indicated by the much stronger reverse ($u < 0$) flow. For both freestream conditions, the normalized density on the centerline increases from about 0.05 to 0.3 with increasing x in the plotted range, which correlates with decreasing values of the mean free path λ. The location where the mean free path is comparable to the size of the Patterson probe given by its diameter $d_P = 3$ mm is $x \approx 60$ mm for $p_0 = 2$ bar and $x \approx 30$ mm for $p_0 = 10$ bar. Hence, the Patterson probe measurements at distances exceeding these values for the corresponding cases were likely conducted under nonfree molecular conditions, where the effect of first collisions can lead to a systematic reduction of the pressure p_P in the Patterson probe (and therefore to a similar behavior of the number flux $\dot{n}_i$) when looking upstream or to a rise of p_P when looking downstream.

In Figs. 5–8, the measured and calculated flux ratio ϕ profiles on the wake centerline at different model distances are shown for the two freestream conditions, $p_0 = 2$ and 10 bar. All experimental

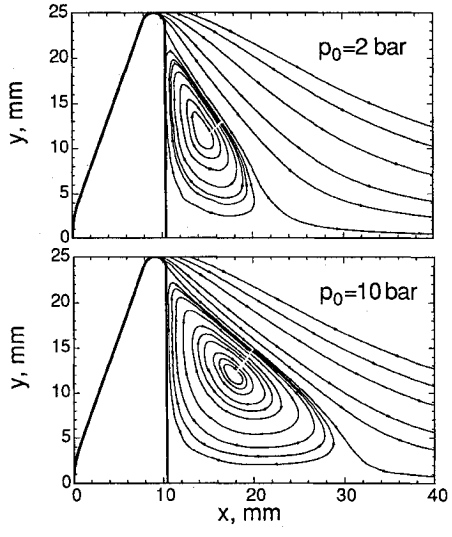

Fig. 3 Streamlines in near wake region.

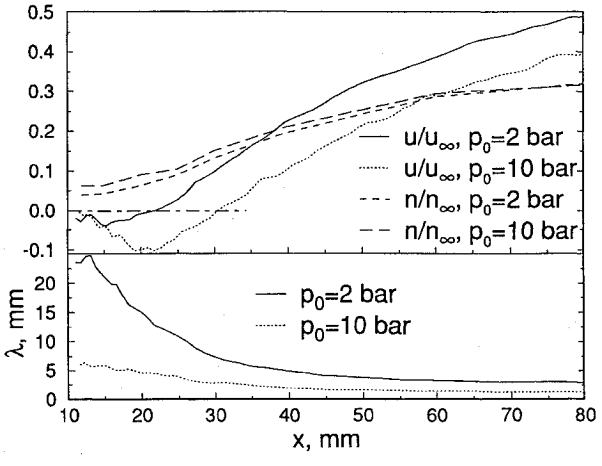

Fig. 4 Mean free path and normalized density and flow velocity along wake centerline.

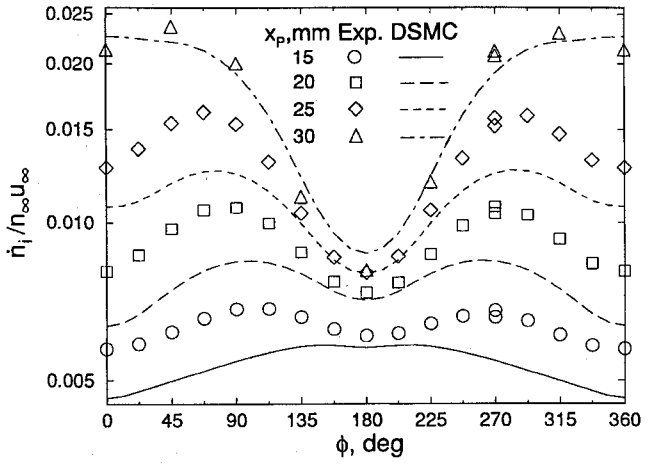

Fig. 5 Flux ratio ϕ profiles on wake centerline, $p_0 = 2$ bar.

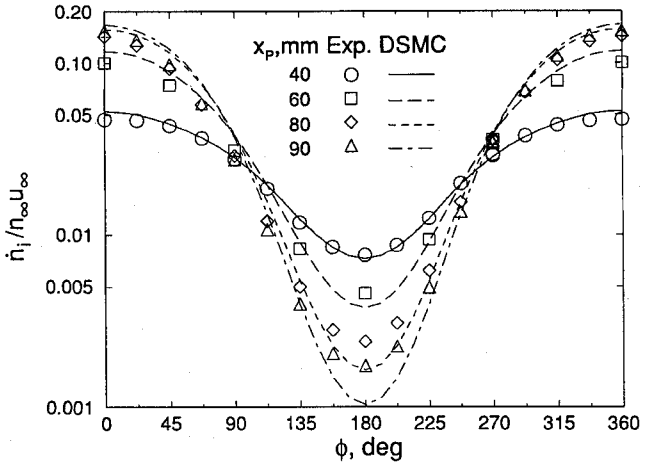

Fig. 6 Flux ratio ϕ profiles on wake centerline, $p_0 = 2$ bar.

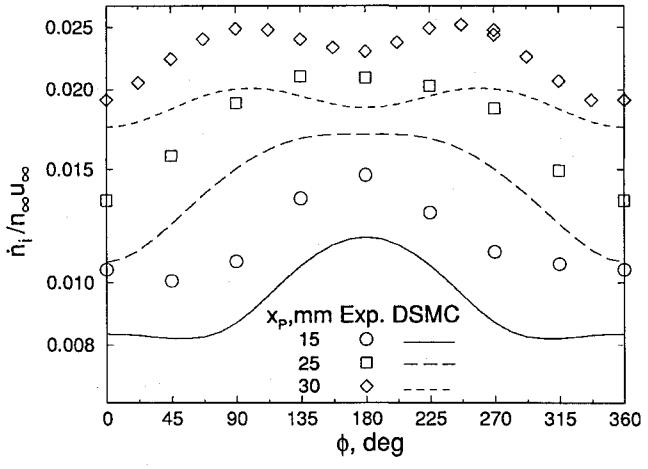

Fig. 7 Flux ratio ϕ profiles on wake centerline, $p_0 = 10$ bar.

profiles are nearly symmetric with respect to the turning angle ϕ as they should be on the symmetry line. The experimental uncertainty can be estimated by the two independently measured values at $\phi =$ 270 deg.

The experimental results for $p_0 = 2$ bar (Figs. 5 and 6) show two relative maxima in the profiles for $x_P \leq 30$ mm (shifting with increasing x_P to $\phi = 0$ and 360 deg), indicating that more molecules are impacting on the probe from the lateral direction of the flow velocity than in direction of this velocity. This appearance of two

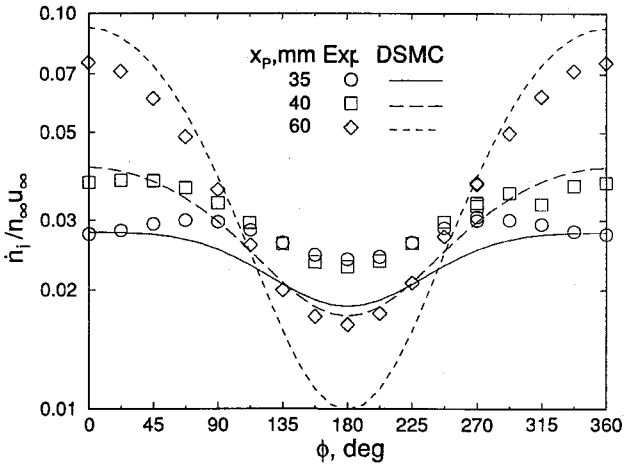

Fig. 8 Flux ratio ϕ profiles on wake centerline, $p_0 = 10$ bar.

maxima cannot be described by a local Maxwellian distribution function, which would give one maximum only in the direction opposite to the flow velocity. At $x_P = 15$ mm the establishment of a vortex is indicated by the relation $\dot{n}_i(\phi = 180\,\text{deg}) > \dot{n}_i(\phi = 0\,\text{deg})$, i.e., reverse flow. The development of the profiles behind the free stagnation point is caused by the increase of the density and the flow velocity with increasing model distance.

The agreement between the experimentally and numerically determined profiles for $p_0 = 2$ bar is good. However, the relative maxima of the calculated profiles are less pronounced and disappear at $x_P = 30$ mm. The calculated profile at $x_P = 15$ mm is based on a relatively small sample size, which might be the reason for the two weak maxima nearly merging. The remaining differences can be explained as follows: For $x_P \leq 25$ mm the calculated number fluxes become smaller (up to 20%) when approaching the $\phi = 0$ deg (or $\phi = 360$ deg) direction, and at $x_P = 20$ mm the calculated ratio $\dot{n}_i$ ($\phi = 0\,\text{deg}$)/$\dot{n}_i$ ($\phi = 180\,\text{deg}$) is smaller than one in contrast to the corresponding experimental value, which means that the calculated reverse flow region is larger than the measured one. The reason for these differences might be the flow disturbance by the Patterson probe: Molecules emerging from the direction of the model can be scattered back by the probe, resulting in an increase of the number density and flux in the nearly free-molecular region between the rear side of the model and the probe (a similar effect was found in the measurements with the dummy probe, where the presence of this probe leads to an increase of the measured number flux from its direction). For $x_P \geq 40$ mm, the systematic deviations, which increase with increasing x_P, can be explained by the expected first collision effects because of the decreasing Knudsen number.

The profiles for $p_0 = 10$ bar (Figs. 7 and 8) are dominated by the strong reverse flow region on the centerline of the wake. At $x_P \leq 30$ mm, the relation $\dot{n}_i$ ($\phi = 0\,\text{deg}$) < $\dot{n}_i$ ($\phi = 180\,\text{deg}$) holds for both the measured and calculated profiles. Two relative maxima at $\phi \approx 90$ and 270 deg can be clearly observed in the measured profiles at $x_P = 30$ and 35 mm; whereas only the calculated profile at $x_P = 30$ mm shows the two maxima, which are, however, less pronounced. The qualitative agreement between the experimental and the numerical results for the profiles in the reverse flow region is good, but the calculated number fluxes are about 10–20% smaller than the measured ones. This discrepancy can be because of the sensitivity of the vortex flow region to either the disturbances by the presence of the Patterson probe or to the physical models implemented in the DSMC procedure. DSMC calculations with the same freestream conditions yield densities that are about 10–15% higher in the vortex region near the centerline of the wake than in our calculations.[5] Behind the free stagnation point, the development of the profiles and the differences between measurements and the DSMC calculations can be explained in the same way as in the case $p_0 = 2$ bar. Because of the smaller mean free paths on the wake centerline, however, the effect of the first collisions starts at smaller distances and is stronger for $p_0 = 10$ bar.

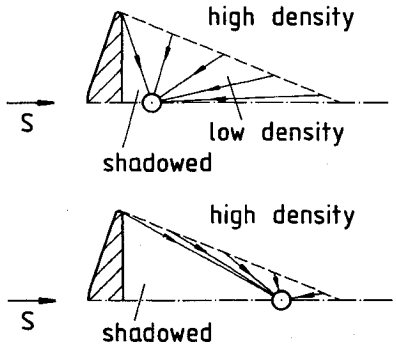

Fig. 9 Direction of molecular fluxes on the axis of a wake (simplified picture).

The overall comparisons between the DSMC results for the number-flux profiles on the wake centerline to the corresponding results of the Patterson probe measurements show a good qualitative and, with some restrictions, quantitative agreement, yielding a mutual validation of the experiments and the calculations. Whether the observed discrepancies are because of experimental or numerical deficiencies can be judged more rigorously by future investigation only, e.g., by density measurements in the wake region or three-dimensional DSMC calculations including the full Patterson probe geometry.

A physical picture of the molecular number fluxes on the centerline in the near-wake region is illustrated in Fig. 9, where the flowfield is simplified by dividing it into one region of high density and another region directly in the wake of nearly free molecular flow (the dividing line could be given by the molecular Mach angle $\mu \approx 1/S$). By molecular scattering, which takes place predominantly in the high-density region, a fraction of the molecules travels from the high-density region through the nearly free molecular region toward the centerline of the wake, thus leading effectively to a number flux emerging from the dividing line. At small distances the shadow angle of the model seen by the Patterson probe is much larger than for large distances, and most molecules are scattered from the backward angles $90\,\text{deg} < \phi < 180\,\text{deg}$. At larger distances, the shadow angle becomes smaller, and the higher velocity of the molecules in the bulk velocity direction will move the angle of the maximum flux to smaller values of ϕ.

The shape of the molecular flow profiles with two relative maxima in the lateral directions can be described in a more realistic way by the assumption of an underlying ellipsoidal distribution function. If $T_\perp > T_\parallel$, then the thermal velocity components perpendicular to the flow direction are larger than the corresponding parallel component, and more molecules can come from the lateral directions. This will be discussed in more detail later.

Distribution Function on the Wake Centerline

Considering the ellipsoidal distribution function Eq. (4) as a suitable approximation of the real distribution function on the centerline, the two speed ratios $S_\perp$ and $S_\parallel$ defined by Eq. (7) with respect to directions perpendicular and parallel to the symmetry axis, respectively, are given by the Patterson probe measurements through Eqs. (8) and (9). The product $n \times u$ is given by Eq. (10). With the determined $S_\perp$, $S_\parallel$, and $n \times u$, the number flux profiles on the wake centerline can be calculated by Eq. (5), which are compared to the corresponding measured profiles in Fig. 10 for $p_0 = 2$ bar. The agreement is remarkably good, which is also true for $p_0 = 10$ bar (Ref. 9). But we must make three annotations. First, the number flux does not contain the whole parameter set and has less information than the underlying ellipsoidal distribution function. Second, the described procedure ensures that the measured and the calculated number flux coincide at the angles $\phi = 0$, 90, and 180 deg; thus the agreement can be regarded as a result of a fitting procedure without much physical basis. Finally, the Patterson probe effectively measures the number flux integrated along the whole entrance plane of the slit with endpoints located at distances ≈2.5 mm from the centerline, where the molecular velocity distribution function might be different from the one on the centerline.

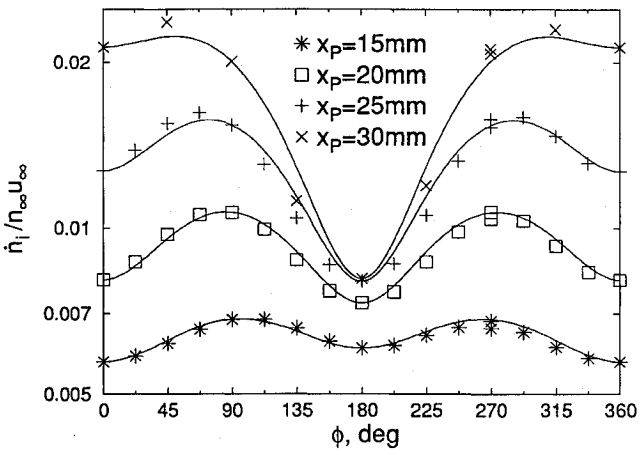

Fig. 10 Number flux ϕ profiles approximated by an ellipsoidal distribution function, $p_0 = 2$ bar.

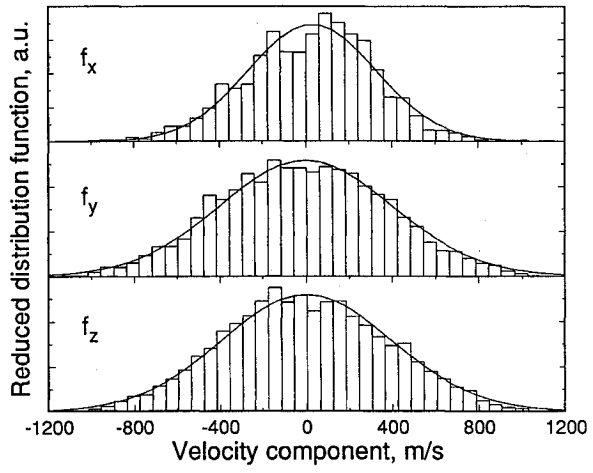

Fig. 11 Sampled and fitted ellipsoidal velocity distribution function, $x_P = 25$ mm, $p_0 = 2$ bar: □, sampled and ——, fitted.

Hence, these experimental results were complemented by sampling the reduced velocity-distribution functions by Eq. (13) in the DSMC calculations in selected cells adjacent to the symmetry axis. In Fig. 11, the sampled distribution functions for each velocity component are compared to the corresponding reduced ellipsoidal distribution functions with parameters derived from nonlinear fitting at $x_P = 25$ mm for $p_0 = 2$ bar, where the number flux profile shows the strongest lateral maxima. The agreement between the sampled and the fitted distribution functions is quite good, which supports the assumption of an approximative description of the distribution function by an ellipsoidal one in this case. The two distribution functions f_y and f_z have nearly the same shape, whereas the width of f_x is significantly smaller, reflecting the nonequilibrium nature of the flow. Corresponding comparisons can also be made at different distances and for $p_0 = 10$ bar, yielding similar results.

Figures 12 and 13 are based on the speed ratios $S_\parallel$ and $S_\perp$ defined by the parameters of the ellipsoidal distribution function either derived from the Patterson probe measurements or from the fits to the sampled distribution functions, where the speed ratio $S_\perp$ derived from the DSMC calculations is the mean value of the corresponding ratios $S_{\perp,y}$ and $S_{\perp,z}$ of the distribution functions f_y and f_z, respectively. For both freestream conditions, the measured values of the speed ratios are clearly greater in the reverse flow region than the ones based on the DSMC results. The most striking difference between the corresponding values of the speed ratios is found at the largest distance $x_P = 90$ mm, where the DSMC values indicate nearly equilibrium conditions (i.e., $S_\parallel \approx S_\perp$); whereas the measured value of $S_\perp$ exceeds the value of $S_\parallel$ by ≈30% for both freestream conditions. Since we can expect an approach to almost equilibrium conditions on the wake centerline with increasing distance from the

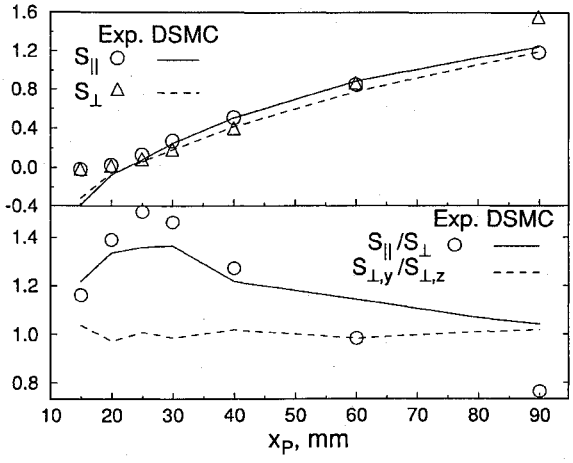

Fig. 12 Experimental and DSMC results for the speed ratios, $p_0 = 2$ bar.

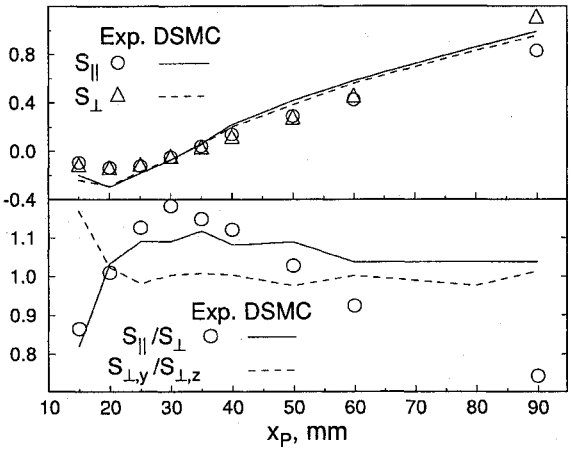

Fig. 13 Experimental and DSMC results for the speed ratios, $p_0 = 10$ bar.

model (as indicated also by the measured values of the speed ratio up to the distance of 60 mm), this deviation might be caused by the systematic error when the Patterson probe is in nonfree molecular supersonic flow.

The degree of nonequilibrium is given by the ratio $S_{||}/S_{\perp}$ (=1 at equilibrium), which is shown as a function of x_P in the lower parts of Figs. 12 and 13. To estimate the statistical errors of the values of the speed ratios fitted to sampled velocity distributions, the ratio $S_{\perp,y}/S_{\perp,z}$ (which should be close to one) is also depicted. Except at the smallest distance for $p_0 = 10$ bar, where there was the smallest sample size, the deviation of this ratio from 1 is always smaller than 3%. Accordingly, a deviation of $S_{||}/S_{\perp}$ from 1 exceeding 3% indicates with significant probability a nonequilibrium condition.

For $p_0 = 2$ bar, the experimental values of $S_{||}/S_{\perp}$ show a single maximum at $x_P = 25$ mm, i.e., near the free stagnation point, where the maximum value of $S_{||}/S_{\perp} \approx 1.5$ indicates a strong nonequilibrium condition. The corresponding DSMC values are about 10% smaller around this maximum, but their qualitative behavior is comparable.

For $p_0 = 10$ bar, the maximum of the experimental values of $S_{||}/S_{\perp}$ is $\approx$1.2, where the location of this maximum coincides again with the location of the free stagnation point at $x \approx 30$ mm. In contrast to the more rarefied $p_0 = 2$ bar condition, this parameter, as well as the corresponding DSMC parameter, drops below the equilibrium value of one at the smallest distance. The DSMC values of $S_{||}/S_{\perp}$ are close to 1.1 within the range 25 mm $\leq x_P \leq$ 50 mm. At larger distances, where the experimental results presumably are influenced by nonfree molecular flow at the Patterson probe, the calculation yields nearly Maxwellian distribution functions, i.e., local equilibrium conditions.

For an ellipsoidal distribution function the inward fluxes $\dot{n}_{i,||}$ and $\dot{n}_{i,\perp}$ through a surface element parallel or perpendicular to the streamlines, respectively, can be calculated by Eq. (5). For $u \ll \zeta_{||}$, where $\zeta_{||,\perp} = \sqrt{(2kT_{||,\perp}/m)}$ are the thermal velocity components, we obtain

$$\dot{n}_{i,||} \approx n\zeta_{||}/2\sqrt{\pi} \quad \text{and} \quad \dot{n}_{i,\perp} \approx n\zeta_{\perp}/2\sqrt{\pi} \tag{14}$$

The relation $S_{||}/S_{\perp} > 1$, which is dominant in the near wake region ($x < 60$ mm) and which is likely caused by the molecular scattering from the high-density region outside the wake into the shadowed region within the wake (cf. Fig. 9), is equivalent to $\zeta_{||} < \zeta_{\perp}$ and, therefore, also to $\dot{n}_{i,||} < \dot{n}_{i,\perp}$, explaining the lateral maxima in the measured and calculated number flux profiles near the free stagnation point, where the condition $u \ll \zeta_{||}$ holds. Because of the lower DSMC values of $S_{||}/S_{\perp}$ for both freestream conditions, these lateral maxima are less pronounced in the calculations. When the absolute value of u increases at larger distances from this stagnation point, the lateral maxima in the number flux profiles are shifted toward the flow direction $\phi = 0$ or 180 deg, depending on the sign of u.

Finally, Fig. 14 shows the experimentally determined product $n \times u$ given by Eq. (10) on the wake centerline as a function of the distance x_P for $p_0 = 2$ and 10 bar. For comparison, present DSMC results and results by Moss et al.[5] are also depicted. Good agreement is obtained for $p_0 = 2$ bar. For $p_0 = 10$ bar the DSMC values of $n \times u$ are significantly higher outside the reverse flow region, where the experimental results can be influenced by nonfree molecular flow.

Flux Profiles Outside the Wake Centerline

The number-flux profiles were also measured and calculated outside the wake centerline, i.e., at $y_P > 0$. An example of these results is presented in Fig. 15 for $p_0 = 2$ bar at $x_P = 15$ mm, $y_P = 10$ and

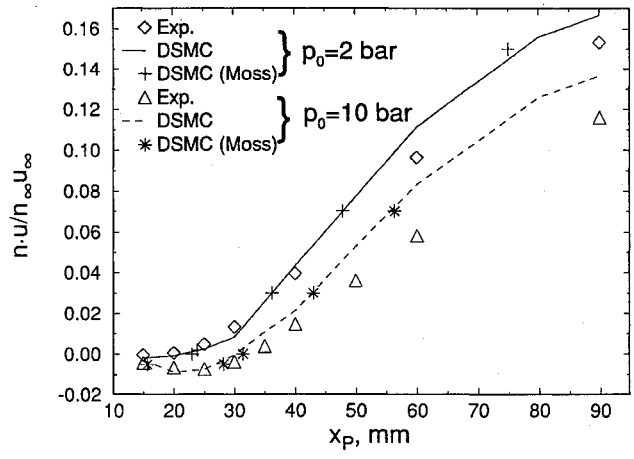

Fig. 14 Experimental and DSMC results for the normalized number flux.

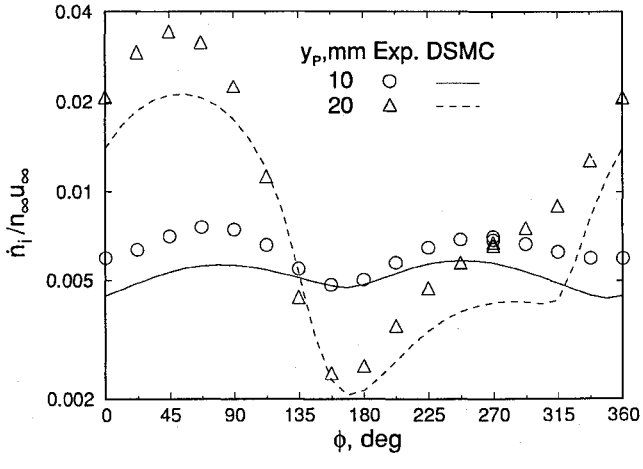

Fig. 15 Flux ratio ϕ profiles outside the wake centerline, $x_P = 15$ mm, $p_0 = 2$ bar.

20 mm, i.e., just below the vortex center and in the free shear layer, as can be surmised from the calculated streamline picture (Fig. 3). The overall qualitative and quantitative agreement between the calculated and the measured profile is good. The measured and the calculated profiles at $y = 10$ mm show two maxima at $\phi \approx 70$ and 250 deg with nearly the same maximum values, indicating strong nonequilibrium conditions. The measured number fluxes are somewhat higher than the calculated ones. This quantitative difference is possibly caused by flow disturbances because of the Patterson probe or by numerical deficiencies in the sensitive vortex region. The profiles at $y_P = 20$ mm are strongly dominated by the radial flow, which results in a strong maximum at $\phi \approx 45$ deg, i.e., opposite to the direction of the flow velocity (cf. Fig. 3).

Concluding Remarks

The Patterson probe measurements in the wake of a 70-deg half-angle cone at Mach numbers $M \approx 16$ and corresponding DSMC calculations show details of the rarefied flow, i.e., of the molecular flux from different directions. A vortex is formed, which increases in length with decreasing Knudsen number. The vortex features are investigated for a small Kundsen number range (2.6×10^{-3}–6.6×10^{-3}), where on the wake centerline the distribution function of the translational degrees of freedom is highly non-Maxwellian and can be approximated by an ellipsoidal distribution function. The comparisons between the DSMC calculations and the present experiments show a good qualitative and, in most cases, also a good quantitative agreement. Consequently, the implication is that the assumptions for the experimental data evaluation—no flow disturbance by the probe, free molecular flow, ratio of transmission probabilities equal one—are sufficient to build a physical picture of the wake flow that is consistent with the DSMC calculations. The range of validity of these assumptions, as well as the sensitivity of the numerical results to different DSMC models and calculation procedures, should be investigated in future studies.

Acknowledgments

The authors thank A. Klotzbach, D. Rammenzweig, and G. von Roden for their help in performing the experiments and the data evaluation. The authors would also like to thank S. Dietrich and I. Boyd for making available the DSMC code MONACO.

References

[1]Anon., *Capsule Aerothermodynamics*, edited by J. Muylaert, AGARD-FDP-VKI Lecture Series 1995-06, von Kármán Inst. for Fluid Dynamics, Rhode Saint Genèse, Belgium, March 1995.

[2]Legge, H., "Experiments on a 70 Degree Blunted Cone in Rarefied Hypersonic Flow," AIAA Paper 95-2140, June 1995.

[3]Kastell, D., Horvarth, T. J., and Eitelberg, G., "Recompression of Nonequilibrium Flow in the Wake of a Blunted Body," *Proceedings of the 20th International Symposium on Shock Waves*, edited by B. Sturtevant, World Scientific Publishing, Singapore (to be published).

[4]Bird, G. A., *Molecular Gas Dynamics and the Direct Simulation of Gas Flows*, Oxford Univ. Press, Oxford, England, UK, 1994.

[5]Moss, J. N., Price, J. M., Dogra, V. K., and Hash, D. B., "Comparison of DSMC and Experimental Results for Hypersonic External Flows," AIAA Paper 95-2028, June 1995.

[6]Patterson, G. N., "Theory of Free-Molecule, Orifice-Type Pressure Probes in Isentropic and Nonisentropic Flows," Inst. of Aerophysics, Univ. of Toronto, UTIA Rept. 412, Toronto, ON, Canada, Nov. 1956.

[7]Hughes, P. C., "Theory for the Free Molecular Impact Probe at an Arbitrary Angle of Attack," Inst. for Aerospace Studies, Univ. of Toronto, UTIAS Rept. 103, Toronto, ON, Canada, May 1965.

[8]Koppenwallner, G., "The Free Molecular Pressure Probe with Finite Slot Orifice," *Proceedings of the 14th Symposium on Rarefied Gas Dynamics*, edited by Ed. H. Oguchi, Vol. 1, Univ. of Tokyo Press, Tokyo, Japan, 1984, pp. 415–422.

[9]Legge, H., "Patterson Probe Measurements in the Wake of a 70 Deg Half Angle Cone in Hypersonic Rarefied Flow," German Aerospace Research Establishment, DLR-IB 223-94 A 15, Göttingen, Germany, Dec. 1994.

[10]Bartz, J. A., and Vidal, R. J., "Experimental Study of Pseudo Transpiration at an Orifice in Rarefied Flow," *Proceedings of the 6th Symposium on Rarefied Gas Dynamics*, edited by L. Trilling and H. Y. Wachmann, Vol. 1, Academic, New York, 1969, pp. 639–653.

[11]Legge, H., "Modelling Free Molecular Plume Flow and Impingement by an Ellipsoidal Distribution Function," *Rarefied Gas Dynamics: Space-Related Studies*, edited by E. P. Muntz, D. P. Weaver, and D. H. Campbell, Vol. 116, Progress in Astronautics and Aeronautics, AIAA, Washington, DC, 1989, pp. 189–203.

[12]Koppenwallner, G., "The Free Molecular Pressure Probe with Finite Length Slot Orifice," German Aerospace Research Establishment, IB 222-84 A 15, Göttingen, Germany, May 1984.

[13]Dietrich, S., and Boyd, I. D., "Parallel Implementation on the IBM SP-2 of the Direct Simulation Monte Carlo Method," AIAA Paper 95-2029, June 1995.

[14]Borgnakke, C., and Larsen, P. S., "Statistical Collision Model for Monte Carlo Simulation of Polyatomic Gas Mixture," *Journal of Computational Physics*, Vol. 18, No. 4, 1995, pp. 405–420.

[15]Bergemann, F., and Boyd, I. D., "New Discrete Vibrational Energy Model for the Direct Simulation Monte Carlo Method," *Rarefied Gas Dynamics: Experimental Techniques and Physical Systems*, edited by B. D. Shizgal and D. P. Weaver, Vol. 158, Progress in Astronautics and Aeronautics, AIAA, Washington, DC, 1994, pp. 174–183.

I. D. Boyd
Associate Editor